Available online at www.sciencedirect.com
SCIENCE DIRECT®
Biochemical and Biophysical Research Communications 334 (2005) 276–287
BBRC
www.elsevier.com/locate/ybbrc

Withanolides, a new class of natural cholinesterase inhibitors with calcium antagonistic properties ☆

M. Iqbal Choudhary [a,*], Sarfraz Ahmad Nawaz [a], Zaheer-ul-Haq [a], M. Arif Lodhi [a], M. Nabeel Ghayur [b], Saima Jalil [a], Naheed Riaz [a], Sammer Yousuf [a], Abdul Malik [a], Anwarul Hassan Gilani [b], Atta-ur-Rahman [a]

[a] *Dr. Panjwani Center for Molecular Medicine and Drug Research, International Center for Chemical Sciences, University of Karachi, Karachi-75270, Pakistan*
[b] *Department of Biological and Biomedical Sciences, The Aga Khan University, Karachi-74800, Pakistan*

Received 4 June 2005
Available online 29 June 2005

Dedicated to the memory of Prof. Abdus Salam (1926–1996), a nobel laureate (1976)

Abstract

The withanolides **1**–**3** and **4**–**5** isolated from *Ajuga bracteosa* and *Withania somnifera*, respectively, inhibited acetylcholinesterase (AChE, EC 3.1.1.7) and butyrylcholinesterase (BChE, EC 3.1.1.8) enzymes in a concentration-dependent fashion with IC_{50} values ranging between 20.5 and 49.2 μM and 29.0 and 85.2 μM for AChE and BChE, respectively. Lineweaver–Burk as well as Dixon plots and their secondary replots indicated that compounds **1**, **3**, and **5** are the linear mixed-type inhibitors of AChE, while **2** and **4** are non-competitive inhibitors of AChE with K_i values ranging between 20.0 and 45.0 μM. All compounds were found to be non-competitive inhibitors of BChE with K_i values ranging between 27.7 and 90.6 μM. Molecular docking study revealed that all the ligands are completely buried inside the aromatic gorge of AChE, while compounds **1**, **3**, and **5** extend up to the catalytic triad. A comparison of the docking results showed that all ligands generally adopt the same binding mode and lie parallel to the surface of the gorge. The superposition of the docked structures demonstrated that the non-flexible skeleton of the ligands always penetrates the aromatic gorge through the six-membered ring A, allowing their simultaneous interaction with more than one subsite of the active center. The affinity of ligands with AChE was found to be the cumulative effects of number of hydrophobic contacts and hydrogen bonding. Furthermore, all compounds also displayed dose-dependent (0.005–1.0 mg/mL) spasmolytic and Ca^{2+} antagonistic potentials in isolated rabbit jejunum preparations, compound **4** being the most active with an ED_{50} value of 0.09 ± 0.001 mg/mL and 0.22 ± 0.01 μg/mL on spontaneous and K^+-induced contractions, respectively. The cholinesterase inhibitory potential along with calcium antagonistic ability and safe profile in human neutrophil viability assay could make compounds **1**–**5** possible drug candidates for further study to treat Alzheimer's disease and associated problems.

Keywords: Withanolides; *Ajuga bracteosa*; *Withania somnifera*; Acetylcholinesterase; Butyrylcholinesterase; Molecular docking studies; Enzyme inhibition; Calcium antagonist

AChE (EC 3.1.1.7) is a key component of cholinergic brain synapses and neuromuscular junctions. The major biological role of the enzyme is the termination of impulse transmission by rapid hydrolysis of the cationic neurotransmitter acetylcholine [1]. According to the cholinergic hypothesis, memory impairments in patients with the senile dementia are due to a selective and irreversible deficiency in the cholinergic functions in the brain [2]. This serves as the rationale for the use of AChE inhibitors for the symptomatic treatment of AD

☆ *Abbreviations:* AChE, acetylcholinesterase; BChE, butyrylcholinesterase; PAS, peripheral anionic site; AD, Alzheimer's disease.

* Corresponding author. Fax: +92 21 4819018, +92 21 4819019.
E-mail address: hej@cyber.net.pk (M.I. Choudhary).

0006-291X/$ - see front matter © 2005 Elsevier Inc. All rights reserved.
doi:10.1016/j.bbrc.2005.06.086

in its early stages. Certain classes of intestinal spasmolytics are known to have a combination of Ca^{2+} antagonist and AChE inhibitory activities. Histamine H_1 blockers like promethazine and mepyramine, and H_2 receptor antagonists such as cimetidine, oxmetidine, and ranitidine have been shown to possess AChE inhibitory potentials [3,4]. The role of BChE (EC 3.1.1.8) in normal aging and brain diseases is still elusive. It has been found that BChE is present in significantly higher quantities in Alzheimer's plaques than that of normal age related non-demented brains [5].

The comprehensive study of the AChE/inhibitor complexes by X-ray crystallography has indicated a nearly identical three-dimensional structure of the active site, located 20 Å from the protein surface at the bottom of a deep and narrow gorge [6]. The different positions of the known inhibitors in the binding pocket suggest that more than one clearly defined binding site exists which are called esteratic and anionic subsites. Esteratic subsite contains catalytic triad (Ser200, His440, and Glu327) [7] and oxyanion hole forming residues (Gly118, Gly119, and Ala201) [8]. The quaternary ammonium-binding locus (Trp84, Phe330, and Glu199) is responsible for binding of the quaternary trimethyl ammonium tail group of ACh by cation–π interaction [9]. The peripheral site, which is also called peripheral anionic site (PAS), includes Tyr70, Asp72, Tyr121, Tyr334, and Trp279 residues [10,11]. Ligand occupation of the peripheral anionic site may allosterically change the conformation of the active center [11]. Aromatic residues lining the gorge and residues, located at the outer rim of the gorge have been postulated to be involved in the initial binding and guiding of the substrate towards the active site [12].

The discovery of natural cholinesterase inhibitors has been a very challenging area of drug development due to the involvement of cholinesterases in Alzheimer's disease and other related dementias. We have previously reported a number of new natural inhibitors of cholinesterases (AChE and BChE) isolated from indigenous medicinal plants [13,14]. The steady-state inhibition kinetics, pharmacological profiles, SAR and 3D-QSAR, CoMFA and CoMSIA [15–17] studies have been conducted on a plenty of compounds. Continuing our program to introduce new drug candidates of Alzheimer's disease, we identified withanolides **1**–**5**, with efficacious cholinesterase inhibitory potential.

The objectives of the current investigation were, first, to identify the cholinesterase inhibitors and then to explore the possible binding modes of these compounds in the active site of AChE by kinetics and molecular docking studies. Second, to establish correlation between AChE inhibition and Ca^{2+} antagonistic potential of compounds **1**–**5** for their therapeutic relevance in AD and finally evaluation of cytotoxicity.

Experimental

The AChE and BChE inhibiting activities were measured by spectrophotometric method developed by Ellman et al. [18]. Electric-eel AChE (EC 3.1.1.7), horse-serum BChE (EC 3.1.1.8), acetylthiocholine iodide, butyrylthiocholine chloride, 5,5′-dithiobis[2-nitrobenzoic acid] (DTNB), and galanthamine were purchased from Sigma (St. Louis, MO, USA). All other chemicals were of analytical grade. Standard operational assay protocol was the same as described previously [19].

The rate of the enzymatic reaction [18] was measured by the following equation:

$$\text{rate (mol/L/min)} = \frac{\text{change in absorbance/min}}{13,600}.$$

All the kinetic experiments were performed in 96-well microtiter-plates by using SpectraMAX 340.

Determination of kinetic parameters

The (IC_{50}) concentration of test compounds that inhibited the hydrolysis of substrates (acetylthiocholine and butyrylthiocholine) by 50% was determined by monitoring the effect of various concentrations of the inhibitors in the assays on the inhibition values. The IC_{50} (inhibitor concentration that inhibits 50% activity of AChE and BChE) values were then calculated using the EZ-Fit Enzyme Kinetics program (Perrella Scientific, Amherst, USA). The interaction of compounds **1**–**5** with AChE and BChE can be described by the following schemes:

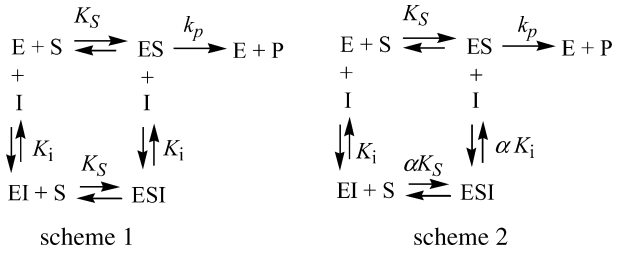

scheme 1 scheme 2

where ES is the AChE–ATCh or BChE–BTCh complex and P is the product. K_i and αK_i are the inhibition constants reflecting the interactions of inhibitors with the free AChE or BChE and the AChE-ATCh or BChE-BTCh complexes, respectively.

Dissociation constant/inhibition constant (K_i) was determined by the interpretation of Dixon plot [20]. Lineweaver–Burk plot [21] and their secondary replots using initial velocities were obtained over a substrate concentration range between 0.1 and 0.4 mM for acetylthiocholine iodide (ATCh) and 0.05–0.2 mM for butyrylthiocholine chloride (BTCh). The dependency of V_{max}/K_m and V_{max} on inhibitor [I] is given by:

$$V_{max}/K_m = \left(\frac{(V_{max}/K_m)K_i}{K_i + [I]}\right) \Rightarrow I = \frac{K_i}{K_i + [I]} \Rightarrow K_i = K_i + [I].$$

Non-linear regression equations were used to determine the values of K_i, K_m, and V_{max} in the Lineweaver–Burk plot and Dixon plots. The K_i value (dissociation constant/inhibition constant of AChE–inhibitor or BChE–inhibitor complex into free AChE or BChE and inhibitor) was determined graphically by Dixon plot and Lineweaver–Burk plots; first, $1/V_{maxapp}$ was calculated at each intersection point of lines of every inhibitor concentration on y-axis of the Lineweaver–Burk plot and then replotted against various concentrations of inhibitor. Second, the slope of each line of inhibitor concentration on Lineweaver–Burk plot was plotted against inhibitor concentrations. Then, replotting slope versus various concentrations of inhibitor, K_i, was the intercept on x-axis.

Statistical analysis

Graphs were plotted using GraFit program [22]. Values of the correlation coefficients, slopes, intercepts, and their standard errors were obtained by the linear regression analysis using the same program. The correlation for all the lines of all graphs was found to be >0.99. Each point in the constructed graphs represents the mean of three experiments.

Molecular docking studies

The three-dimensional structures of ligands were constructed and optimized using the SYBYL program [23]. Energy minimization was performed using the tripos force field with a distance gradient algorithm with convergence criterion of 0.05 kcal/(mol Å) and maximum 1000 interactions, respectively. The FlexX [24] method was applied to dock ligands with most of the default parameters, in the aromatic gorge of AChE complexed with decamethonium (PDB id; 1ACL). A radius of 6.5 Å was used to define the active-site interaction points. FlexX software is a fast and flexible algorithm for docking small ligands in binding sites of the enzymes, using an incremental construction algorithm that actually builds the ligands in the binding site [23]. The software incorporates protein–ligand interactions, placement of the ligand core, and rebuilding the complete ligand. Docking results were analyzed by VMD [25] and LIGPLOT [26]. All the computational studies were performed by using computer server on a dual processor 1.5 GHz Intel-based PC running the LINUX SUSE 8.2 (Kernel 2.4) operating system.

Spasmolytic and calcium antagonist activities

Antispasmodic activity of the compounds **1**–**5** was studied in isolated spontaneously contracting rabbit jejunum [27]. Rabbits from a local breed of both sexes (1.5–2.0 kg) were obtained from the animal house of the Aga Khan Medical University (Karachi). Standard operational protocol has been described previously [28].

Under these experimental conditions, the rabbit jejunum exhibited spontaneous rhythmic contractions and therefore allowed the study of the relaxant (spasmolytic) activity directly without the use of an agonist. Calcium antagonist activity was confirmed by the ability of the compounds **1**–**5** to relax the high K^+ (80 mM)-induced contraction.

Cytotoxic evaluation

Isolation of human neutrophils. Heparinized fresh venous blood was drawn from healthy volunteers in a local blood bank and the neutrophils were isolated by the method of Siddiqui et al. [29]. The isolation neutrophils have been described elsewhere [28].

Assay procedure. Isolated human neutrophils (1×10^7 cells/mL) were incubated first with test compounds for 30 min and then by the addition of 0.25 mM WST-1 (Dojindo Laboratories, Kumamoto, Japan) in water bath shaker at 37 °C [30]. After 3 h incubation, change in the absorbance was measured at 450 nm in 96-well plate by using SpectraMAX 340 (Molecular Devices, CA, USA). The OD is the mean of the five experimental replicates. The percentage (%) cell viability was calculated by using the following formula:

$$\text{percentage viability of cells} = \{(\text{OD test compound} \times 100/\text{OD control}) - 100\} - 100.$$

Results and discussion

Withanolides **1**–**5**, isolated from *Ajuga bracteosa* [31] and *Withania somnifera* [32], possess an erogstane skeleton with lactone ring (Chart 1). The cholinesterase inhibitory potential of these withanolides was measured by using electric-eel (*Torpedo californica*) (1ACL) AChE. Oligomeric forms of electric-eel AChE are similar to those of vertebrate's nerve and muscle AChE [6]. Moreover, results of studies on this enzyme can be correlated with molecular modeling studies by the coordinates of eel AChE X-ray structure. Horse-serum BChE has similarities with synaptic AChE in primary amino acid sequence, deduced secondary structure, and active-site chemistry; the two enzymes also have overlapping specificities for substrates and inhibitors [33].

Compounds **1**–**5** inhibited acetylcholinesterase (AChE; EC 3.1.1.7) and butyrylcholinesterase (BChE, EC 3.1.1.8) enzymes in a concentration-dependent manner with K_i values ranging between 20.0 and 45.0 and 27.7–90.6 μM for AChE and BChE, respectively. K_i values were calculated by three different methods: first, the slopes of each line in the Lineweaver–Burk plot were plotted against different concentrations of inhibitors; second, the $1/V_{maxapp}$ was calculated by plotting different fixed concentrations of substrate (ATCh or BTCh) versus ΔV in the presence of different fixed concentrations of inhibitors in the respective assays of AChE or BChE. Then, K_i was calculated by plotting different concentrations of inhibitor versus $1/V_{maxapp}$, K_i was the intercept on the x-axis. In the third method, K_i was directly measured from Dixon plot as an intercept on x-axis. Determination of the inhibition type is important in understanding the mechanism of inhibition and the sites of inhibitor binding. Lineweaver–Burk plot, Dixon plots, and their replots indicated that compounds **1**, **3**, and **5** have linear mixed-type of inhibition for AChE as in these cases there were decrease in V_{max} values with the increase of K_m. Generally, this type of inhibition is the combination of partial competitive and pure non-competitive type of inhibition. On the other hand, **2** and **4** exhibit pure non-competitive type of inhibition for AChE, as in these cases there were decreases in V_{max} without affecting the affinity (K_m values) of the AChE or BChE towards the substrate (ATCh or BTCh), respectively. In other words, inhibitor and ATCh or BTCh bind randomly and independently at the different sites of AChE or BChE, respectively. It also indicated that the inhibition depends only on the concentration of inhibitor and dissociation constant (K_i). Similarly, all compounds **1**–**5** were found to be the pure non-competitive inhibitors of BChE. The K_i, K_m, K_{maxapp}, V_{max}, V_{maxapp}, V_{maxapp}/K_m, IC_{50} values and the type of inhibition have been presented in Table 1. The graphical analysis of steady-state inhibition data of compounds **1** and **2** for AChE has been shown in Fig. 1. Compounds **5** ($K_i = 21.0 \pm 0.1$ μM) and **2** ($K_i = 27.7 \pm 0.1$ μM) were found to possess strong binding with AChE and BChE, respectively. Similarly, compounds **3** ($K_i = 45.0 \pm 0.1$ μM) and **5** ($K_i = 90.6 \pm 0.02$ μM) displayed weak binding with AChE and BChE, respectively.

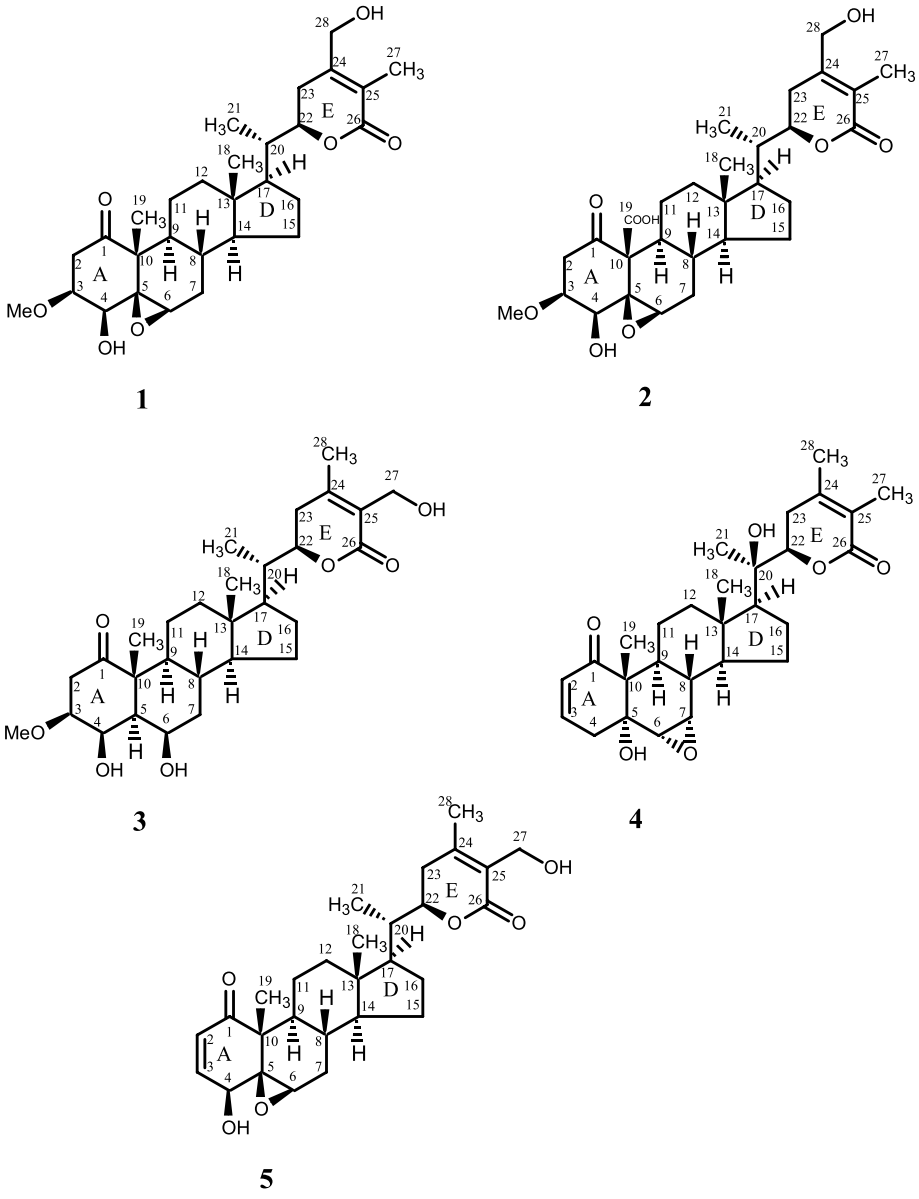

Chart 1. Structures of compounds **1**–**5**.

In order to predict the interactions of compounds **1**–**5** in the aromatic gorge of AChE (*T. californica*), docking positions with the lowest energy were achieved, indicating that the phase space has been sufficiently sampled. Docking protocol for each ligand was repeated many times and best docking positions with their respective minimum energies were consistently reproduced. The size and shape of this series of ligands supported a gorge-spanning binding mode. Therefore, AChE co-crystallized with decamethonium was taken as a model, for comparison in order to monitor the performance of our docking approach employed in this study.

The best ranking docking solutions showed that AChE could accommodate compounds **1**–**5** ideally inside the aromatic gorge. Comparison of the docking results with aliphatic bis-quaternary inhibitors such as decamethonium and/or aromatic ring containing inhibitors such as BW284C51 [34] shows that compounds **1**–**5** could not penetrate deep into the aromatic gorge like these inhibitors rather remain close to the anionic subsites. This might be due to the bulky skeleton of compounds **1**–**5** as compared to BW284C51 and decamethonium known inhibitors of AChE. Compounds **1**–**5** orient themselves along the active-site gorge in such a way that their activity can be attributed only to different substituents at these ligands. Like DME999 [34], compounds **1**–**5** span the entire AChE surface (Fig. 2) with possibility of multiple-binding sites. The superimposition of the decamethonium ligand in the crystal structure of the complex (PDB entry 1ACL) with our results shows that decamethonium enters relatively deeper into the aromatic gorge than our new inhibitors. A

Table 1
Kinetic parameters from steady-state inhibition data of AChE and BChE in the presence of compounds **1–5**

Enzymes	Compounds	IC_{50} (μM) ± SEM	K_i (μM) ± SEM	K_m (μM)	K_{mapp} (μM)	V_{max} (μmol/L/min)	V_{maxapp} (mean) (μmol/L/min)	V_{maxapp}/K_m (min/U)	Type of inhibition
AChE	**1**	25.2 ± 0.1	23.0 ± 0.1	0.12	0.20	5.0	2.1	17.6	Mixed-type
	2	22.1 ± 0.2	20.8 ± 0.2	0.12	0.12	5.0	2.2	18.3	Non-competitive
	3	49.2 ± 0.1	45.0 ± 0.1	0.12	0.19	5.0	2.0	16.6	Mixed-type
	4	45.2 ± 0.2	40.5 ± 0.05	0.12	0.12	5.0	2.3	19.1	Non-competitive
	5	20.5 ± 0.1	20.0 ± 0.1	0.12	0.120	5.0	2.5	20.0	Mixed-type
	Galanthamine[a]	0.5 ± 0.001	0.45 ± 0.001	0.12	0.18	5.1	2.6	21.6	Mixed-type
BChE	**1**	38.4 ± 0.01	39.3 ± 0.05	0.31	0.31	8.0	4.2	13.5	Non-competitive
	2	29.0 ± 0.02	27.7 ± 0.1	0.31	0.31	8.0	4.3	13.8	Non-competitive
	3	40.0 ± 0.04	36.5 ± 0.01	0.31	0.31	8.0	4.0	12.9	Non-competitive
	4	45.1 ± 0.01	46.1 ± 0.01	0.31	0.31	8.0	3.9	12.5	Non-competitive
	5	95.2 ± 0.02	90.6 ± 0.02	0.31	0.31	8.0	4.0	12.9	Non-competitive
	Galanthamine[b]	8.5 ± 0.01	8.0 ± 0.01	0.31	0.30	8.1	4.2	13.5	Non-competitive

[a,b] Standard inhibitors of AChE and BChE, K_i values (dissociation constant or inhibition constant) were determined from non-linear regression analysis by Dixon plot and secondary Lineweaver–Burk plot at various concentrations of compounds **1–5**, K_m (Michaelis–Menten constant) is equal to the reciprocal of x-axis intersection, V_{max} (maximal velocity) is equal to the reciprocal of y-axis intersection of each line for each concentration of compounds **1–5** in the Lineweaver–Burk plot. The V_{maxapp} is equal to the reciprocal of y-axis intersection of each line for each concentration of compounds **1–5** in Dixon plot (each point in Lineweaver–Burk represents the mean of three determinations).

comparison of the docking results of all five ligands showed that all compounds generally adopt the same binding mode. This similar binding mode is not surprising, as all the ligands have almost same structure with minor difference of functional groups (Chart 1). The superposition of the docked structures clearly demonstrates that the non-flexible skeleton of the ligands always penetrates the aromatic gorge through the six-membered ring A. Thus, ring A is placed at the bottom of the gorge that might be due to the apparently greater hydrophobicity of ring A as compared to the five-membered ring D (Figs. 3 and 4). The compounds **1**–**5** under study were found to be completely buried inside the aromatic gorge of the AChE (see Fig. 2). This position contributes to the stabilization of the AChE-ligand complexes, as the backbones of the ligands are highly hydrophobic due to their carbocyclic character. The principal interactions holding the ligands **1**–**5** in the active site of AChE (*T. californica*) are summarized as follows.

*Compound **1**–AChE complex*

Ligand **1** has interaction with all the four subsites of the active center of AChE (Fig. 5). Ser200 forms hydrogen bond (3.0 Å) with the carbonyl oxygen of ring A. Similarly, side chain carbon has hydrophobic contact with ring A. In addition to hydrogen bonding, compound **1**–AChE complex is also stabilized by the hydrophobic contacts with PAS (Tyr121, Trp279) residues of AChE. Trp279, located at the top of the gorge, is thought to have the ability to regulate entry of ligand **1** into the gorge. Furthermore, compound **1** also holds hydrophobic interactions with acyl-binding locus (Phe290, Phe331) and choline-binding site (Trp84, Glu199, and Phe330). In case of decamethonium only amino acid residues of Phe331, His440, Gly441, Trp84, Trp279, and Tyr70 of AChE have hydrophobic contacts with the ligand. BW284C51 and E2020 bind through their two-phenyl and quaternary amino end-groups complexed to Trp84 and Phe330 (choline-binding) [34]. The affinity ($K_i = 23.0 \pm 0.1$ μM) of compound **1** with AChE may be the cumulative effect of hydrogen bonding along with hydrophobic contacts with all the subsites of the active center, due to the interactions with all the four subsites of the active-site mixed-type of inhibition exhibited by ligand **1** is not unexpected.

*Compound **2**–AChE complex*

Ligand **2** binds at anionic subsites and thus hinders access to esteratic site (Fig. 5). Amino acid residues of PAS and choline-binding pocket of AChE play a key role in the stabilization of compound **2**–AChE complex. Tyr70 forms hydrogen bond (3.2 Å) with carboxyl group oxygen of ring B, while residues of Tyr121, Tyr334, and Tyr279 interacted with the ligand through

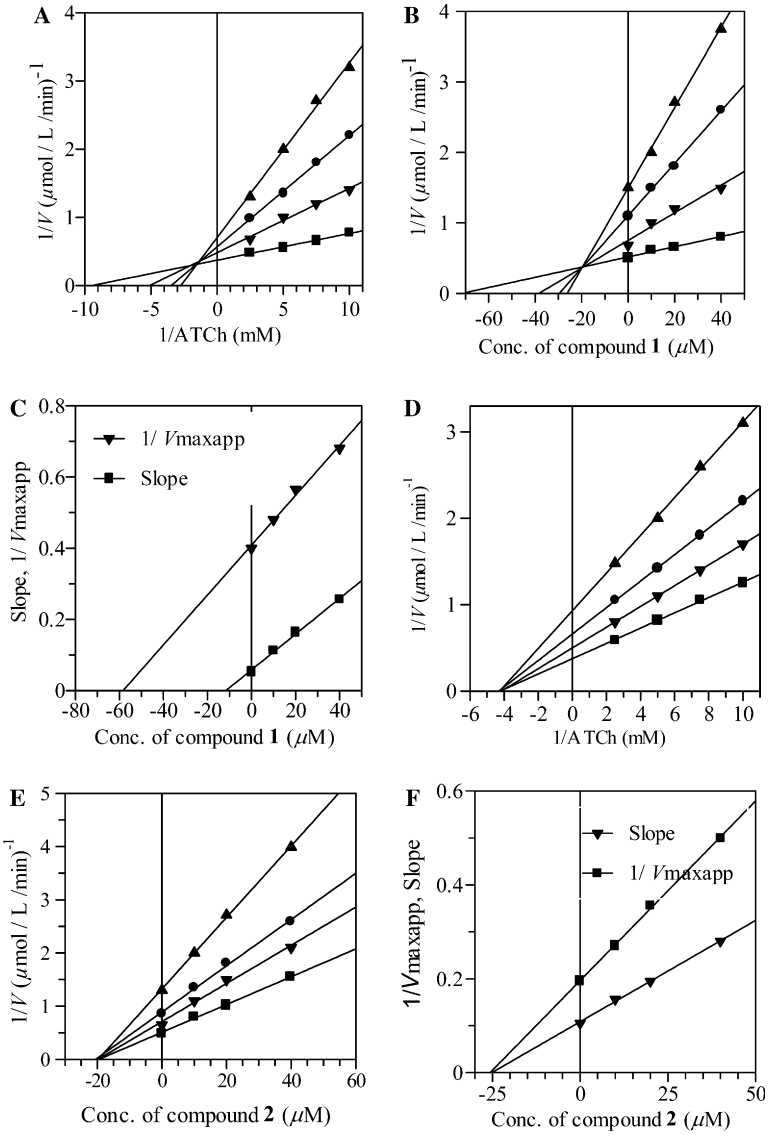

Fig. 1. Steady-state inhibition of AChE by compounds **1** and **2**. (A) The Lineweaver–Burk plot of reciprocal of initial velocities versus reciprocal of four fixed ATCh concentrations in absence (■) and presence of 10.0 μM (▼), 20.0 μM (●), 40.0 μM (▲) of compound **1**. (B) The Dixon plot of reciprocal of the initial velocities versus various concentrations of compound **1** at fixed ATCh concentrations, (■) 0.4 mM, (▼) 0.2 mM, (●) 0.133 mM, and (▲) 0.1 mM. (C) The secondary replot of the Lineweaver–Burk plot, $1/V_{maxapp}$ or slope versus various concentrations of compound **1**. (D) The Lineweaver–Burk plot of reciprocal of initial velocities versus reciprocal of four fixed ATCh concentrations in absence (■) and presence of 10.0 μM (▼), 20.0 μM (●), 40.0 μM (▲) of compound **2**. (E) Dixon plot of reciprocal of the initial velocities versus various concentrations of **2** at fixed ATCh concentrations, (■) 0.4 mM, (▼) 0.2 mM, (●) 0.133 mM, and (▲) 0.1 mM. (F) The secondary replot of the Lineweaver–Burk plot, $1/V_{maxapp}$ or slope versus various concentrations of compound **2**.

hydrophobic interactions. Similarly, Tyr130 in choline-binding region forms hydrogen bond (2.8 Å) with methoxy oxygen of ring E, while Trp84 has π–π stacking that is energetically favorable to stabilize compound **2**–AChE complex. Similarly, Glu199 is also strongly involved in hydrophobic contacts. This residue is assumed to make concave type of binding site that recognizes the quaternary ammonium function. Gly117 and Gly118 can form peptide bonds with both compound **2**–AChE and free AChE [35]. The oxyanion hole formed by the backbone NH groups of Gly118, Gly119, and Ala201 plays a critical role in stabilizing the structures of the transition states and lowers the activation barriers of AChE catalyzed ATCh hydrolysis. An interesting observation seen in compound **2**–AChE complex is the flip of the peptide bond between Gly117 and Gly118. As a consequence, the position of the main chain nitrogen of Gly118 in the oxyanion hole is occupied by the carbonyl group of Gly117. This renders the oxyanion hole less accessible to substrate and less capable of stabilizing its tetrahedral intermediate for nucleophilic attack by Ser200. Furthermore, the flipped conformation can be stabilized by Gly117 that forms hydrogen bonds with Gly119 and Ala201, suggesting that the flip of the

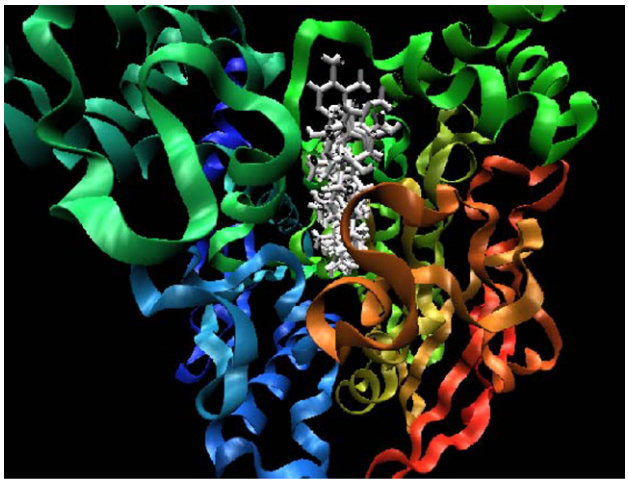

Fig. 2. Showing that the ligands **1**–**5** are completely buried inside the aromatic gorge of the AChE (*T. californica*).

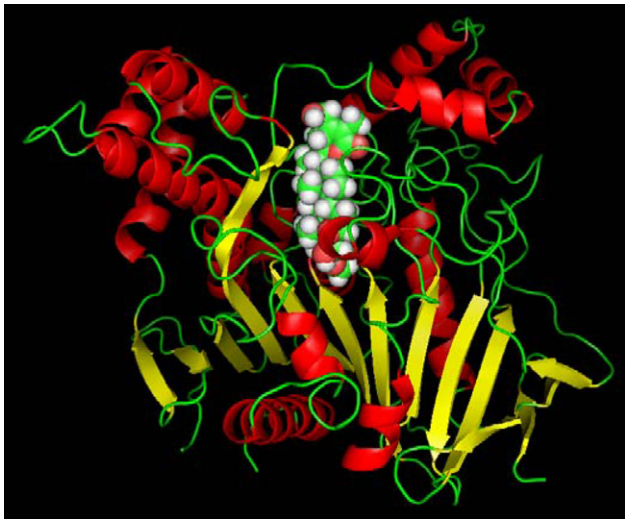

Fig. 3. A view showing that ligand **1** is completely buried inside the aromatic gorge of the AChE (*T. californica*). Helix (red), sheet (yellow), and loop (green).

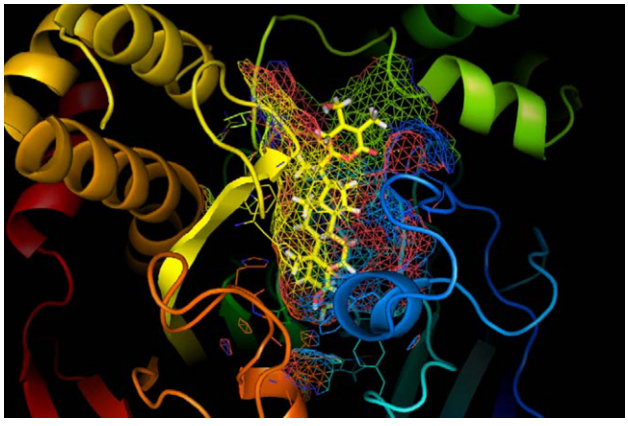

Fig. 4. Another view of ligand **1** in the gorge, showing that it is completely buried inside the aromatic gorge, penetrating deep into the gorge of the AChE (*T. californica*). Helix (red), sheet (yellow), and loop (green).

Gly117–Gly118 peptide bond should be an intrinsic property of AChE. Ligand **2** binds on anionic subsites and has no access to the esteratic site, indicating non-competitive type of inhibition, which is in agreement with steady-state inhibition data (Table 1). Compound **2** ($K_i = 20.8 \pm 0.2$ μM) has a strong binding with the AChE as compared to compound **1** ($K_i = 23 \pm 0.1$ μM) that may be due to the strong hydrogen bonding and hydrophobic contacts in compound **2**–AChE complex.

Compound 3–AChE complex

Compound **3**–AChE complex is stabilized through the interactions involving all the four subsites of the active center. Ser200 (catalytic residue) forms hydrogen bond (2.8 Å) with carbonyl oxygen of ring A. PAS (Tyr121, Trp279) has hydrophobic contacts with rings D and E near the entrance of the active site. Choline-binding pocket amino acid residues (Trp84, Glu199, and Phe330) interact near the bottom of the gorge while acyl-binding locus (Phe331) interacts with C and side chain methyl group near the center of the gorge, respectively. As previous study has revealed that proper positioning of the Glu199 carboxylate relative to the catalytic triad can play a key role in defining its functional role in the interaction of AChE with substrates and inhibitors. In complexes involving compounds **1** and **3**, Glu199 has hydrophobic interaction in the vicinity of catalytic residues near the bottom of the gorge. While in the compound **2**–AChE complex, it has interaction with ring E near the entrance of the gorge of AChE. That may be favorable for the higher activity of the compound **2**–AChE complex. The low inhibitory potential of compound **3** ($K_i = 45.0 \pm 0.01$ μM) than **2** ($K_i = 20.8 \pm 0.2$ μM) may be attributed due to less hydrophobic contacts and hydrogen bonding in compound **3**–AChE complex than in compound **2**–AChE complex. Steady-state inhibition data and docking results are in good agreement with each other, suggesting mixed-type of inhibition of compound **3**–AChE complex.

Compound 4–AChE complex

Tyr121 is forming hydrogen bonds with epoxide oxygen (3.1 Å) at ring B and hydroxyl group (2.6 Å) present at the junction of rings A and B. PAS residues of AChE (Asp72, Tyr334, and Trp279) are involved in hydrophobic contacts. Similarly, compound **4** has hydrophobic interactions with residues of the acyl-binding locus (Phe290 and Phe331) and choline-binding pocket (Phe330) near the bottom and middle of the gorge, respectively. Unique feature of compound **4**–AChE complex is that epoxide oxygen forms hydrogen bond with Tyr121, while in other AChE–ligand complexes, reported in this article, no such type of bond formation

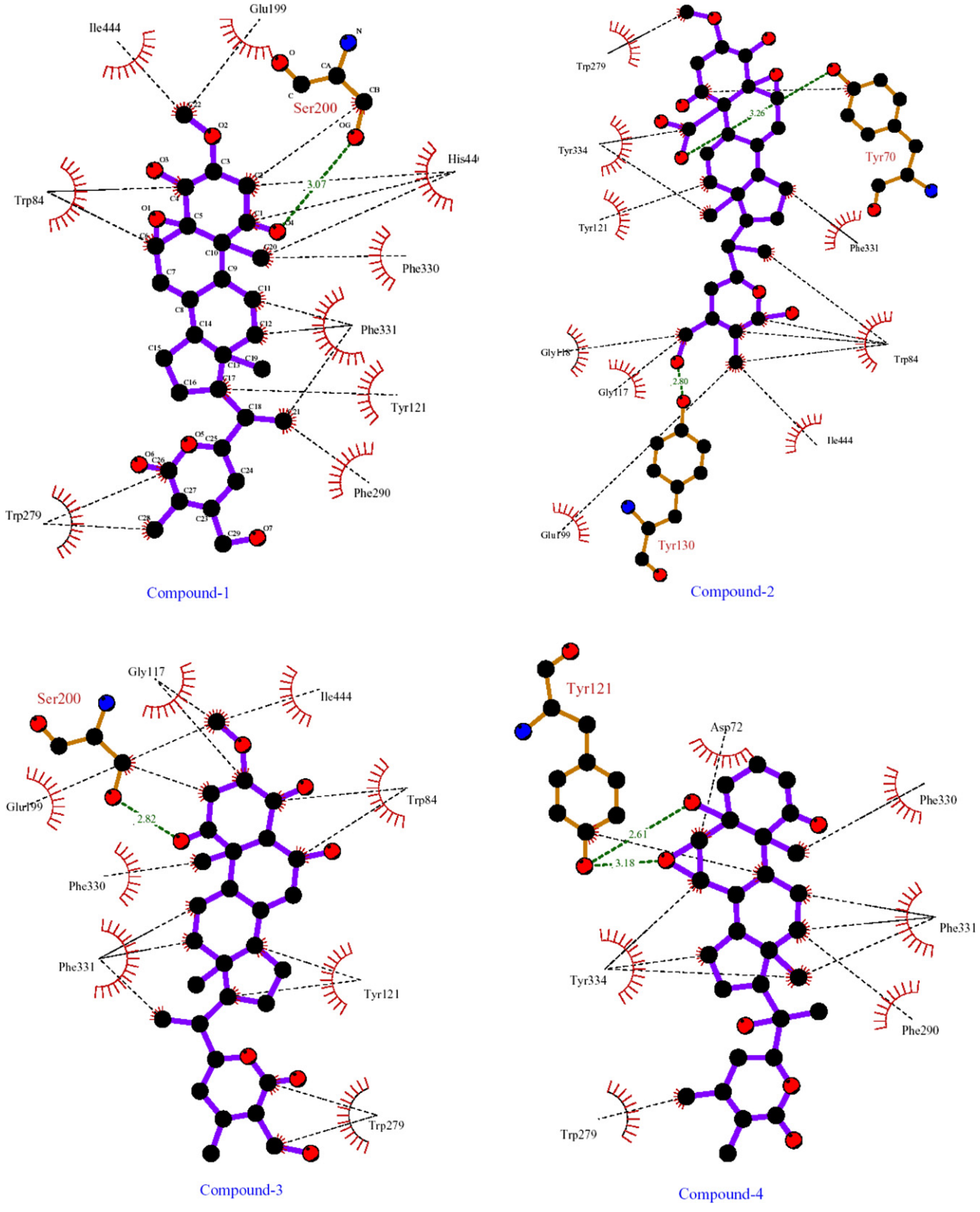

Fig. 5. 2D-Schematic representation of compounds **1**–**5** by LIGPLOTS, showing that hydrophobic contacts and hydrogen bonding are the principal interactions, holding the ligand–receptor complexes in stable form.

with epoixde has occurred. This may be due to the fact that in compound **4**–AChE complex epoxide is present at position C-6/C-7 of ring B, having α-orientation and due to less operational steric hindrance it can form hydrogen bond easily, while in other AChE–inhibitor complexes it is β-oriented and cannot easily form

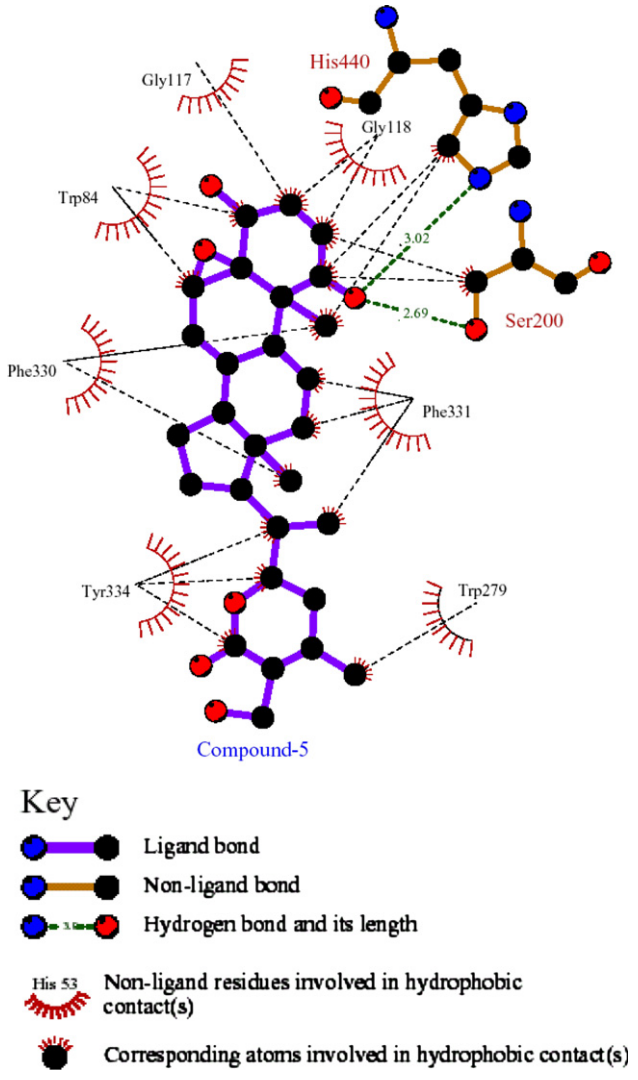

Fig. 5. (*continued*)

hydrogen bonds with the amino acid residues present in the vicinity. Same is true with the hydroxyl group present at the junction of the rings A and B in ligand **4**. Similarly, interactions with the Asp72 were observed only in compound **4**–AChE complex. Asp72 of AChE (*T. californica*) located at the boundary between the PAS and the acylation site (active site) is a key residue with which the ligands can interact. Previous study revealed that Asp72 contributes very little to electrostatic effect to the cationic ligands [36]. However, experiments of kinetics did not provide the atomic details for the role Asp72 plays when compound **4** enters or leaves the active-site gorge. As a negatively charged residue at the entrance of the deep gorge, Asp72 may generate electrostatic field affecting the cationic substrates or inhibitors. Asp72 does not often directly contact with these ligands, but can form water bridges with ligands leaving and entering the AChE-binding gorge acting as clamp to compound **4** and place into the active site [37]. The lower inhibitory potential ($K_i = 40.5 \pm 0.05$ μM) of compound **4** may be due to the less hydrophobic contacts although Tyr121 makes two hydrogen bonds which may be due to unfavorable conformational changes of the ligand with the receptor.

Compound 5–AChE complex

Compound **5**–AChE complex is stabilized through the interactions with all the four subsites of the active center resulting in the mixed-type of inhibition, which is in agreement with steady-state inhibition data. In compound **5**–AChE complex, carbonyl oxygen of the ligand at ring A forms strong hydrogen bonds with catalytic triad residues Ser200 (2.0 Å) and His440 (3.0 Å). Compound **5** also experiences hydrophobic interactions near the entrance of the cavity with PAS (Trp279, Tyr334) residues of AChE. Choline-binding pocket (Phe330, Trp84) and acyl-binding locus (Phe331) residues also have hydrophobic contacts with ring C and chain methyl group side chain of ligand **5**. The higher inhibitory potential ($K_i = 20.0 \pm 0.1$ μM) of compound **5** may be due to strong hydrogen bonding and hydrophobic interactions. Due to the interactions with all the four subsites of the active center of AChE, mixed-type of inhibition is predicted.

Previous evidences also suggest that the AChE may play a key role in the development of AD plaques by accelerating β-amyloid (Aβ) deposition [38] and molecules able to interact exclusively with PAS or with both catalytic and PAS-binding sites can prevent the proaggregating activity of AChE towards Aβ [39–41]. Therefore, compounds **1**–**5**, PAS binding and with catalytic triad-binding AChE inhibitors, might represent a new therapeutic option, as these compounds should be able to overcome the cognitive deficiency and to avoid Aβ aggregation.

In isolated tissue experiments, compounds **1**–**5** caused dose-dependent (0.003–1.0 μg/mL) relaxation of spontaneously contracting rabbit jejunum (Table 2), compound **4** being the most active with median effective

Table 2
ED_{50} values of the compounds **1**–**5** for their spasmolytic effect on spontaneously contracting and high K^+-contracted isolated rabbit jejunum preparations

Compounds	Spontaneous (mg/mL)	High K^+(mg/mL)
1	0.28 ± 0.01	0.88 ± 0.03
2	0.17 ± 0.00	0.70 ± 0.04
3	0.26 ± 0.01	0.44 ± 0.05
4	0.09 ± 0.00	0.22 ± 0.06
5	0.23 ± 0.01	0.85 ± 0.09

Compound **4** showed the highest activity with ED_{50} values of 0.09 ± 0.00 and 0.22 ± 0.001 μg/mL on spontaneous and K^+-induced contractions, respectively (values shown are means ± SEM of three experimental determinations).

Table 3
Viability of human neutrophils (1×10^7 cells/mL) in the presence of 200 μg/mL concentration of withanolides **1**–**5**

Compounds	Viability (%)
1	96.0 ± 2.9
2	95.5 ± 4.0
3	94.3 ± 3.6
4	94.2 ± 3.0
5	98.6 ± 2.0
Galanthamine[a]	96 5 ± 2 5

[a] Positive control, mean ± SD of three experiments.

dose (ED_{50}) of 0.09 ± 0.001 μg/mL (mean ± SEM; $n = 3$). When tested for their possible mode of spasmolytic action, compounds **1**–**5** were also able to relax the high K^+ (80 mM)-induced contraction. Compound **4** again showed the highest potential with an ED_{50} value of 0.22 ± 0.01 μg/mL (mean ± SEM; $n = 3$), indicating the Ca^{2+} antagonistic potential. Verapamil, a standard calcium antagonist, has exhibited a similar effect with an ED_{50} of 0.2 ± 0.04 μg/mL (mean ± SEM; $n = 3$). It is a well-known fact that changes in the calcium homeostasis contribute towards aging, resulting in higher cortical functions as calcium ions maintain a nexus between membrane excitation and subsequent intracellular enzymatic responses [42]. Verapamil and nifedipine like calcium antagonist have also been shown to be effective in preventing old age dementia and Alzheimer's disease mainly due to the role played by calcium in modulating brain functions [43,44]. The proclaimed hypothesis is to prevent calcium overload, particularly in damaged neurons. The mechanism of cell loss in AD may involve an influx of calcium that causes neuronal dysfunction and/or neuronal death. By influencing neurotransmitter balance and preventing excessive elevation of intracellular neuronal calcium levels, compounds **1**–**5** might be expected to prolong cell survival and improve cell function.

In order to evaluate the toxic effects of compounds **1**–**5** on human neutrophils, a standard operational protocol with galanthamine as positive control was developed. Galanthamine is an AChE inhibitor and is used as a drug for the treatment of Alzheimer's disease. The viability of human neutrophils (1×10^7 cells/mL) in the presence of 200 μg/mL of compounds **1**–**5** has been presented in Table 3. From the results (Table 3), it is clear that compounds **1**–**5** have safe profile of human neutrophil viability assay and possess non-toxic nature like that of galanthamine.

Conclusions

This study was focused to identify the cholinesterase inhibitors isolated from medicinally important plants and to explore their possible binding modes in the active site of AChE by kinetics and molecular docking studies. We discovered that withanolides **1**, **3**, and **5** were linear mixed-type of AChE inhibitors, while compounds **2** and **4** were found to be non-competitive inhibitors of AChE. All **1**–**5** compounds were found to be non-competitive inhibitors of BChE. Molecular docking study revealed that all are completely buried in the aromatic gorge of AChE, they are not as deep as decamethonium. That might be due to the bulky skeleton of these ligands. They have almost similar binding mode, which was not unexpected as all the ligands have similar structure with different functional groups. AChE–ligand complexes in this class of compounds are mainly stabilized through hydrophobic interactions and hydrogen bonding, especially with the amino acid residues of PAS of AChE. As β-amyloid aggregating property of AChE during the early stages of AD can be inhibited by non-competitive or mixed-type of inhibitors can prevent the proaggregating activity of AChE towards Aβ. Therefore, compounds **1**–**5**, PAS binding and/or with catalytic triad-binding AChE inhibitors, might represent a new therapeutic option, as these compounds should be able to overcome the cognitive deficiency and to avoid Aβ aggregation.

Therefore, it can be concluded that strong interactions of compounds **1**–**5** with the PAS or with both PAS and catalytic triad residues of AChE indicate high inhibitory potential against AChE and consequently AChE-induced β-amyloid aggregation. Furthermore, compounds **1**–**5** also showed dose-dependent spasmolytic and Ca^{2+} antagonistic activities in isolated rabbit jejunum preparations. That can be helpful in preventing the excessive elevation of intracellular neuronal calcium level, and prolonging the cell survival and function. Thus, we can say that the Ca^{2+} antagonistic potential combined with cholinesterase inhibitory activities and safe profile in human neutrophils viability assay could make compounds **1**–**5** candidates for further study to treat Alzheimer's disease and associated problems. Furthermore, the observed binding modes of compounds **1**–**5** in the active site of AChE explain the affinities of a series of withanolides and thus can provide a rational basis for the structure-based drug design with improved pharmacological properties.

Acknowledgments

The authors express their gratitude to the Higher Education Commission (HEC) and Ministry of Science and Technology, Government of Pakistan, for providing the financial support under the Pak-Kazakh Scientific Co-operation program. We are extremely grateful to Prof. Dr. Rafat Ali Siddiqui (Methodist Research Institute, University of Indianapolis, USA) for his useful suggestions and meaningful discussions during his visit

to our enzyme inhibition laboratory under the TOK-TEN program. Authors are also pleased to acknowledge Prof. Dr. Bernd M. Rode (Department of Theoretical Chemistry, University of Innsbruck, Austria) for his valuable support in molecular docking studies.

References

[1] D.M. Quinn, Acetylcholinesterase: enzyme structure, reaction dynamics, and virtual transition states, Chem. Rev. 87 (1987) 955–979.
[2] E.K. Perry, The cholinergic hypothesis-ten years on, Br. Med. Bull. 42 (1986) 63–69.
[3] G. Bertaccini, G. Couruzzi, H_2-receptor antagonists: side effects and adverse effects, Ital. J. Gastroenterol. 16 (1984) 119–125.
[4] G. Kounenis, D. Voutsas, M.K. Papadopoulou, V. Elezoglou, Inhibition of acetylcholinesterase by the H_2-receptor antagonist nizatidine, J. Pharmacobiodyn. 11 (1988) 767–771.
[5] S.Q. Yu, H.W. Holloway, T. Utsuki, A. Brossi, N.H. Greig, Synthesis of novel phenserine-based-selective inhibitors of butyrylcholinesterase for Alzheimer's disease, J. Med. Chem. 42 (1999) 1855–1861.
[6] J.L. Sussman, M. Harel, F. Frolow, C. Oefiner, A. Goldman, L. Toker, I. Silman, Atomic structure of acetylcholinesterase from *Torpedo californica*: a prototypic acetylcholine-binding protein, Science 253 (1991) 872–879.
[7] M. Harel, D.M. Quinn, H.K. Nair, I. Silman, J.L. Sussman, The X-ray structures of transition state analog complex reveal that molecular origin of the catalytic power of the substrate specificity of acetylcholinesterase, J. Am. Chem. Soc. 118 (1996) 2340–2346.
[8] T. Szegletes, W.D. Mallender, T.L. Rosenberry, Non-equilibrium analysis alters the mechanistic interpretation of inhibition of acetylcholinesterase by peripheral site ligands, Biochemistry 37 (1998) 4206–4216.
[9] M. Harel, I. Schalk, L. Ehret-Sabatier, F. Bouet, M. Goeldner, C. Hirth, P.H. Axelsen, I. Silman, J.L. Sussman, Quaternary ligand binding to aromatic residues in the active-site gorge of acetylcholinesterase, Proc. Natl. Acad. Sci. USA 90 (1993) 9031–9035.
[10] A. Shafferman, A. Ordentlich, R. Barak, C. Kronman, T. Ber, N. Bino, R. Ariel, B. Velan, Electrostatic attraction by surface charge does not contribute to the catalytic efficiency of acetylcholinesterase, EMBO J. 13 (1994) 3448–3455.
[11] Z. Radic, R. Zduran, D.C. Vellom, Y. Li, C. Cervenasky, P. Taylor, Site of the faiculin interaction with acetylcholinesterase, J. Biol. Chem. 269 (1994) 11233–11239.
[12] Atta-ur-Rahman, S. Parveen, A. Khalid, A. Farooq, M.I. Choudhary, Acetyl and butytrylcholinesterase-inhibiting triterpenoid alkaloids from *Buxus papillosa*, Phytochemistry 58 (2001) 963–968.
[13] Atta-ur-Rahman, Zaheer-ul-Haq, F. Feroz, A. Khalid, S.A. Nawaz, M.R. Khan, M.I. Choudhary, New cholinesterase-inhibiting steroidal alkaloids from *Sarcococca saligna*, Helv. Chem. Acta 87 (2004) 439–448.
[14] Atta-ur-Rahman, F. Feroz, S.A. Nawaz, M.R. Khan, M.I. Choudhary, New Pregnan-type steroidal alkaloids from *Sarcocca saligna* and their cholinesterase inhibiting activity, Steroids 69 (2004) 735–741.
[15] A. Khalid, M.I. Choudhary, Zaheer-ul-Haq, S. Anjum, M.R. Khan, Atta-ur-Rahman, Kinetics and structure–activity relationship studies on steroidal alkaloids that inhibit cholinesterases, Bioorg. Med. Chem. 12 (2004) 1995–2003.
[16] Zaheer-ul-haq, B. Wellenzohn, K.R. Liedl, B.M. Rode, Molecular-docking studies of natural cholinesterase-inhibiting steroidal alkaloids from *Sarcococa saligna*, J. Med. Chem. 46 (2003) 5087–5090.
[17] Zaheer-ul-haq, B. Wellenzohn, S. Tonmunphean, A. Khalid, M.I. Choudhary, B.M. Rode, 3D-QSAR studies on natural acetylcholinesterase inhibitors of *Sarcococa saligna* by comparative molecular field analysis (CoMFA), Bioorg. Med. Chem. Lett. 13 (2003) 4375–4380.
[18] G.L. Ellman, K.D. Courtney, V. Andres, R.M. Featherstone, A new and rapid colorimetric determination of acetylcholinesterase activity, Biochem. Pharmacol. 7 (1961) 88–95.
[19] M.I. Choudhary, K.P. Devkota, S.A. Nawaz, F. Shaheen, Atta-ur-Rahman, New cholinesterase inhibiting steroidal alkaloids from *Sarcococca hookeriana* of Nepalese origin, Helv. Chem. Acta 87 (2004) 1099–1108.
[20] M. Dixon, The determination enzyme inhibitors constant, Biochem. J. 5 (1953) 170–171.
[21] I.H. Segel, Non-competitive inhibition (simple intersecting linear non-competitive inhibition), in: Enzyme Kinetics: Behavior and Analysis of Rapid Equilibrium and Steady-State Enzyme Systems, Wiley, New York, 1993, pp. 101–112.
[22] R.J. Leatherbarrow, GraFit Version 4.09, Erithacus Software Ltd., 1999.
[23] K. Stains, SYBYL molecular modeling software. Tripos Associate Ltd., St. Louis, MO, 1999.
[24] M. Rarey, B. Kramer, T. Lengauer, G. Klebe, A fast flexible docking method using an incremental construction algorithm, J. Mol. Biol. 261 (1996) 127–134.
[25] W. Humphrey, A. Dalke, K. Schulten, "VMD—Visual molecular dynamics, J. Mol. Graph. 14 (1996) 33–38.
[26] A.C. Wallace, R.A. Laskowski, J.M. Thornton, LIGPLOT: a program to generate schematic diagrams of protein–ligand interactions, Protein Eng. 8 (1995) 127–134.
[27] A.H. Gilani, K.H. Janbaz, M. Zaman, A. Lateef, S.R. Tariq, H.R. Ahmed, Hypotensive and spasmolytic activities of crude extract of *Cyperus scariosus*, Arch. Pharm. Res. 17 (1994) 145–149.
[28] M.I. Choudhary, S.A. Nawaz, Zaheer-ul-Haq, M.K. Azim, M.N. Ghayur, M.A. Lodhi, S. Jalil, A. Khalid, A. Ahmed, B.M. Rode, Atta-ur-Rahman, A.H. Gilani, V.U. Ahmad, Juliflorine: a potent natural peripheral anionic-site-binding inhibitor of acetylcholinesterase with calcium-channel blocking potential, a leading candidate for Alzheimer's disease therapy, Biochem. Biophys. Res. Commun. 332 (2005) 1171–1179.
[29] R.A. Siddiqui, D. English, Y. Cui, M.I. Martin, J. Wentlands, L. Akard, J. Thompson, J.G.N. Garcia, Phorbol ester-induced priming of superoxide generation by phosphatidic acid-stimulated Neutrophils and granule-free neutrophil cytoplasts, J. Leukoc. Biol. 58 (1995) 189–195.
[30] V. Michael, N. Berridge, S. Tan, D. Kathy, R. Wang, The biochemical and cellular basis of cell proliferation assay that use tetrazolium salts, Biochemica 4 (1996) 14–19.
[31] N. Riaz, A. Malik, Aziz-ur-Rehman, P. Muhammad, S.A. Nawaz, M.I. Choudhary, Cholinesterase inhibiting withanolides from *Ajuga brateosa*, Chem. Biodiversity 1 (2004) 1289–1295.
[32] M.I. Choudhary, S. Yousuf, S.A. Nawaz, S. Ahmed, Atta-ur-Rahman, New cholinesterase inhibiting withanolides from *Withania somnifera*, Chem. Pharm. Bull. 52 (2004) 1358–1361.
[33] M. Arpagaus, A. Chatonnet, P. Masson, M. Newton, T.A. Vaughan, C.F. Bartels, C.P. Nogueira, La.B.N. Du, O. Lockridge, Use of the polymerase chain reaction for homology probing of butyrylcholinesterase from several vertebrates, J. Biol. Chem. 266 (1991) 6966–6974.
[34] E. Felder, M. Harel, I. Silman, J.L. Sussman, Structure of a complex of the potent and specific inhibitor BW284C51 *Torpedo californica* acetylcholinesterase, Acta Crystallogr. D 58 (1991) 872–879.

[35] M.L. Raves, M. Harel, Y.P. Pang, I. Silman, A.P. Kozikowski, J.L. Sussman, 3 D structure of acetylcholinesterase complexed with the neotropic alkaloid, (−) huperzine A, Nat. Struct. Biol. 4 (1997) 57–63.
[36] Z. Radic, P.D. Kirchhoff, D.M. Quinn, J.A. McCammon, P. Taylor, Electrostatic influence on the kinetics of ligand binding to acetylcholinesterase. Distinctions between active center ligands and fasciculin, J. Biol. Chem. 272 (1997) 23265–23277.
[37] Y. Xu, J. Shen, X. Luo, I. Silman, J.L. Sussman, K. Chen, H. Jiang, How does huperzine A enter and leave the binding gorge of acetylcholinesterase? Steered molecular dynamics simulations, J. Am. Chem. Soc. 125 (2003) 11340–11349.
[38] H. Soreq, S. Seidman, Acetylcholinesterase—new roles of an old actor, Nat. Rev. Neurosci. 2 (2001) 294–302.
[39] N.C. Instrosa, A. Alvarez, C.A. Perez, R.D. Moreno, M. Vicente, C. Linker, O.I. Casanueva, C Soto, J. Garrido, Acetylcholinesterase accelerates assembly of amyloid-beta-peptides into Alzheimer's fibrils: possible role of the peripheral site of the enzyme, Neuron 16 (1996) 881–891.
[40] G. Ferrari, V.De. Canales, M.A. Shin, I.L.M. Weiner, I. Silman, N.C. Inestrosa, A structural motif of acetylcholinesterase that promotes amyloid beta peptide fibril formation, Biochemistry 40 (2001) 10447–10457.
[41] M. Bartolini, C. Bertucci, V. Cavrini, V. Andrisano, Beta-amyloid aggregation induced by human acetylcholinesterase inhibition studies, Biochem. Pharmacol. 65 (2003) 407–416.
[42] J. Birks, Nimodipine for primary degenerative, mixed and vascular dementia, The Cochrane Database of Systematic Reviews 1 (2001) CD000147
[43] D.J. Triggle, Biochemical and pharmacological differences among calcium channel antagonists: clinical implications, in: M. Epstein (Ed.), Calcium Antagonists in Clinical Medicine, Hanley and Belfus, Philadelphia, 1992, pp. 1–28.
[44] W. Vagnucci, W. Li, Alzheimer's disease and angiogenesis, Lancet. 361 (2003) 605–608.